Journal of the Ceramic Society of Japan 117 [1] 6-14 2009 **Special Article: Review**

Diffusion of Li atoms in $LiMn_2O_4$ – A structural point of view –

Nobuo ISHIZAWA† and Kenji TATEISHI*

Nagoya Institute of Technology, Asahigaoka, Tajimi, Gifu, 507−0071
***Gifu Prefectural Ceramics Research Institute, Tajimi, Gifu, 507−0811**

The structure of $LiMn_2O_4$, its phase transition at around 290 K, and the diffusion mechanism of Li are discussed based on the recent synchrotron X-ray diffraction and molecular dynamics simulation studies. The high-temperature modification (cubic $Fd\bar{3}m$) is essentially of spinel-type containing various types of disorder; (1) the Li atoms are not located exactly at the tetrahedral 8*a* sites, but mainly distributed among four positions 0.14 Å apart from 8*a*, (2) some portion of Li atoms are further displaced toward the 16*c* octahedral interstices with a notable accumulation at the positions 0.35 Å apart from 16*c*, and (3) the O atoms also show a statistical distribution around their ideal 32*e* sites. The low-temperature modification adopts a $3 \times 3 \times 1$ superstructure (orthorhombic *Fddd*) with respect to the high-temperature modification. The bond-length fluctuation has been observed along the pseudo-tetragonal Jahn–Teller distortion direction parallel to the *a* axis in the heterocubane $Mn2_4O9_4$ cluster. The four Mn2 atoms in the heterocubane presumably shares three electrons in the *e*-parentage low-energy-level orbitals by the double-exchange Zener mechanism. The time-averaged oxidation state for Mn2 is estimated to be +3.25. The heterocubane Zener polarons are isolated with each other and embedded in an ordered way in the charge-ordered matrix containing $Mn1^{III}$, $Mn3^{III}$, $Mn4^{IV}$ and $Mn5^{IV}$. Two kinds of diffusion mechanisms for Li atoms are proposed for the high-temperature modification from the molecular dynamics simulation. One is a microscopic version of the classical picture for diffusion based on the concentration difference in diffusion species. This mechanism requires an activation energy of ca. 0.25 eV to jump over a saddle point at the bottleneck. The other mechanism is a diffusion accompanied by the local lattice distortion coupled with the 3*d* electron transfer between a pair of nearby Mn atoms. This requires no activation energy for Li to pass through the bottleneck. The valence exchange between +3 and +4 in the neighboring Mn pair prompts the displacement of coordinating O atoms along the pseudo-tetragonal Jahn–Teller distortion direction, which presumably plays a principal role in opening the bottleneck of oxygen triangle along the diffusion pathway.

Key-words : Lithium diffusion, Electron density distribution, Zener polaron, Bond length fluctuation, Partial charge ordering, Phase transition, Molecular dynamics simulation, Synchrotron X-ray single-crystal diffraction

[Received September 5, 2008]

1. Introduction

Recent developments of rechargeable lithium ion batteries for electronic devices have stimulated systematic surveys of various candidate materials. Among them the lithium manganese oxides with the spinel-type structure have attracted much attention because of their cost-effectiveness, low toxicity and relatively high energy density when used as positive electrode materials.[1)–4)] In contrast with the energetic surveys and extensive studies of new positive electrode materials, the nature of the Li diffusion in these substances is not well known.

The archetypal $LiMn_2O_4$ crystallizes in the cubic $Fd\bar{3}m$ structure ($a \approx 8.2$ Å) composed of a cubic-close-packing of O atoms in which the Li and Mn atoms occupy a part of tetrahedral and octahedral interstices.[5)] On the basis of the origin choice 2 for $Fd\bar{3}m$ (the inversion centre at the origin), the O atom is located at 32*e* site (x,x,x) with $x \approx 0.26$. Here, the number 32 is multiplicity and *e* is the Wyckoff letter in $Fd\bar{3}m$. The O atom is surrounded by one Li and three Mn atoms tetrahedrally. The Li atom is located at 8*a* site (1/8,1/8,1/8), surrounded by four O atoms tetrahedrally. The Mn atom is located at 16*d* site (1/2, 1/2,1/2), surrounded by six O atoms octahedrally.

A slice of the structure parallel to (–110) is shown in **Fig. 1**, indicating a presence of a one-dimensional chain of edge-sharing MnO_6 octahedra running parallel to [110] to which LiO_4 tetrahedra are attached. These tetrahedra form a zigzagging chain along the dashed line. The zigzagging chain intersects the octahedral 16*c* interstices which are the largest spatial voids in the spinel structure. The zigzagging chains are connected with each other

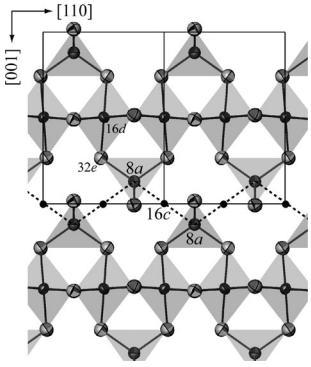

Fig. 1. (–110) slice of the $LiMn_2O_4$ spinel structure composed of edge-shared MnO_6 octahedra and LiO_4 tetrahedra with Li at 8*a*, Mn at 16*d*, and O at 32*e* in the space group $Fd\bar{3}m$. The diffusion pathway of Li is shown as a dashed line connecting tetrahedral 8*a* sites and octahedral 16*c* interstices (black circle). The atomic displacement parameter ellipsoids are plotted at the 90% probability level.

† Corresponding author: N. Ishizawa; E-mail: ishizawa@nitech.ac.jp

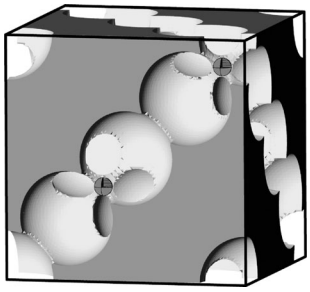

Fig. 2. Cavity drawing of the spinel structure featuring the connected 16*c* octahedral interstices and Li atoms at 8*c* sites. The 16*c* interstices are visualized as spherical cavities of 1.6 Å in diameter.

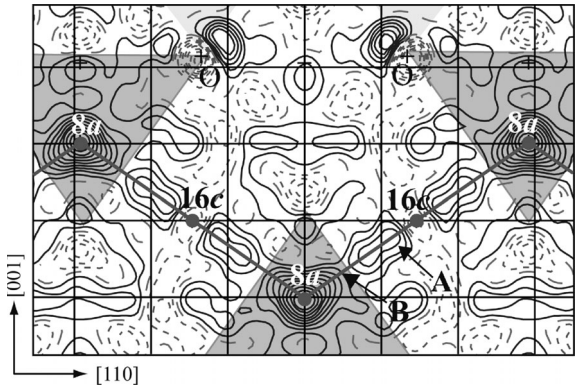

Fig. 3. Difference Fourier map on (–110) near the 8*a*-16*c*-8*a* zigzagging diffusion pathway showing positional disorder of Li and O atoms. Parts of Li atoms are considered to be located near the A and B positions in addition to the regular 8*a* site. Contour intervals are 0.5 e/Å^3. The square grids are drawn with 1 Å intervals for the view purpose. The LiO_4 tetrahedra are shown in pale gray.

to form a three-dimensional tunnel as shown in **Fig. 2**. The conventional understanding of the Li diffusion in $LiMn_2O_4$ is that the Li ions hop over the 8*a* and 16*c* sites in the tunnel with a driving force arising from the concentration difference in Li.[6)]

It is expected, however, that a flexible local structural distortion accompanies the mobile species as it migrates through the structure. The distortion should be most prominent when it passes through the bottleneck of the diffusion tunnel. As will be discussed in section 8, the bottleneck opening in $LiMn_2O_4$ is slightly smaller than the ionic radii of Li based on the concept of effective ionic radii.[7)] The rigidity of the $[Mn_2O_4]^{-1}$ matrix as shown in Fig. 2 can be thus questioned.[8)]

$LiMn_2O_4$ is believed to be a mixed valence compound comprised of two distinct Mn^{III} and Mn^{IV} species in equal proportions. The crystal undergoes a first order structural phase transition at around 290 K.[9)–15)] The transition includes partial charge ordering on the octahedrally coordinated Mn sites.[11)] It was reported from the NMR experiments on $Li[Mn_{1.96}Li_{0.04}]O_4$ that Li is present at 8*a*, 16*c* and 16*d* sites and that Li diffusion occurs in the high temperature phase but not in the low temperature phase.[16)] The latter suggests that the Li ion dynamics and the charge ordering on Mn sites can be closely correlated.

This review first describes the nature of disorder in $LiMn_2O_4$ based on the recently published works using synchrotron X-ray diffraction and molecular dynamics simulation, and then discusses the Li diffusion mechanism to which the dynamical change in oxidation state of Mn is highly correlated.[17)–23)]

2. Structure of the high-temperature phase

The electron density distribution of the high temperature modification was investigated by the synchrotron X-ray powder diffraction using the $Li(Mg_{1/6}Mn_{11/6})O_4$ powders[17)] at beamline 20B, Photon Factory, KEK. The synchrotron X-ray single-crystal diffraction using $LiMn_2O_4$[20)] was carried out on a high-speed horizontal-type four-circle diffractometer[24)] at beamline 14A, Photon Factory, KEK. The use of an eight-channel avalanche photodiode photon-counting detector with a counting linearity of up to 10^8 cps eliminated the use of absorbers and attenuators.[25)] The (–110) difference Fourier map obtained from the synchrotron powder diffraction experiment is shown in **Fig. 3**, where the contribution of Li atoms to the calculated structure factor has been eliminated to bring the disordered distribution of Li atoms in relief. Although the single-crystal experiments showed a higher sensitivity in detecting structural disorders, the main features were essentially the same as the powder experiment. The X-ray diffraction studies revealed several features about the disorder as summarized below.

1) The electron density around Li extends its lobe toward <111>, suggesting a possible large anharmonicity of the Li atom vibration, or an existence of positional disorder, which can be modeled by a statistical distribution among the four positions 0.14 Å displaced from 8*a* along <111>.

2) The electron density around the O atom extends its lobe toward directions perpendicular to <111>, suggesting a possible large anharmonicity of the O atom vibration, or an existence of disorder which can be modeled by a statistical distribution among the three 96*g* sites slightly displaced from 16*c*.

3) The residual electrons form a peak at 0.35 Å apart from 16*c* along the line connecting 8*a* and 16*c*. This suggests that a small amount of constituent atoms are displaced from their ideal positions. It is noted that the displacements usually have an offset from 16*c*.

The X-ray diffraction analysis assumes that atomic geometry and properties of each unit cell in a crystal are exactly the same. This often makes it difficult to distinguish the time- and space-dependent phenomena. By this reason, two possible models, one based on the anharmonicity of thermal vibration and the other based on the statistical distribution of atoms, were examined through the molecular dynamics simulation, which will be described in section 5.

3. Structure and electron density distribution of the low temperature modification

Structure of the low-temperature modification was investigated by the synchrotron X-ray diffraction technique using the $LiMn_2O_4$ single crystal grown by the flux method.[20)] The phase transition brings about a $3 \times 3 \times 1$ superstructure at low-temperatures, compared with the $1 \times 1 \times 1$ cubic unit cell of the high-temperature modification. Repeated measurements using the imaging-plate 3-circle diffractometer revealed that the superstructure reflections appeared at 294(1) K on cooling and disappeared at 310(1) K on heating for the flux-grown $LiMn_2O_4$.[20)]

The structure determination was carried out at 297(1) and 230(1) K on a crystal kept at a low temperature for a long time using a high-speed horizontal-type four-circle diffractometer at beamline 14A, KEK-PF. A large improvement in precision was attained compared with the neutron and X-ray powder diffraction experiments in the literature. The low-temperature modification

is orthorhombic *Fddd*, a = 24.7550(9), b = 24.8832(9), c = 8.2003(3) Å, Z = 72. Numbers of crystallographically independent atom sites in a unit cell are 4 for Li (Li1–Li4 sites), 5 for Mn (Mn1–Mn5 sites) and 9 for O (O1–O9 sites). The unit cell volume exceeds 5000 $Å^3$, which is very large in contrast to most inorganic compounds. Without the use of the fast four-circle diffractometer in combination with the intense synchrotron X-ray flux, it was difficult to determine the electron density distribution to identify the positional disorder of such light elements as Li and O.

Differences in atomic positions between the high- and low-temperature modifications are subtle but significant. The shape of Mn-bearing oxygen octahedra, Mn–O bond distances, and bond valence sums (BVSs) revealed a partial charge ordering in the low-temperature modification, as first indicated by Rodriguez-Carvajal, et al.[11] The BVS's are 3.06 (Mn1), 3.34 (Mn2), 3.12 (Mn3), 3.89 (Mn4) and 3.88 (Mn5). Each Mn1 and Mn3 has a pair of long bonds in body-diagonal direction, suggesting that the *e*-parentage orbitals of the t^3e^1 electron configuration of Mn^{III} are undegenerate in association with the pseudo-tetragonal Jahn–Teller distortion. On the other hand, Mn4 and Mn5 have no such typical difference in the bond distances in each MnO_6 octahedron. It was concluded that the Mn1 and Mn3 sites are occupied by Mn^{III} while the Mn4 and Mn5 sites by Mn^{IV}.

Compared with Mn1, Mn3, Mn4 and Mn5, the oxidation state of Mn at Mn2 site is complicated. The four $Mn2O_6$ octahedra cap all the faces of the tetrahedral void in the spinel structure, as shown in **Fig. 4**. The BVS for Mn2 was 3.34, which is intermediate between +3 and +4, and relatively close to +3. The $Mn2O_6$ octahedra also have a pseudo-tetragonal distortion similar to $Mn1O_6$ and $Mn3O_6$ while the magnitude of the distortion in $Mn2O_6$ is small compared with those in $Mn1O_6$ and $Mn3O_6$. Another peculiarity is that the O9 atoms along the pseudo-tetragonal Jahn–Teller distortion axis showed an apparently large anisotropy in the atomic displacement parameter ellipsoid, as shown in Fig. 4(a).

The low-temperature experiments at 297 and 230 K revealed that the largest atomic displacement parameter for O9 along the a axis did not show any temperature dependency. The cross section of the electron density distribution of O9 at 297 K along the line connecting Mn2 and O9 is asymmetric, as shown in Fig. 4(b).[21] The asymmetric profile was found to be interpreted as a 3:1 sum of two Gaussian profiles of the O atom distribution centered at 2.24 and 1.98 Å from Mn2, respectively. The long distance of 2.24 Å corresponds approximately to the long Mn^{III}-O bond length along the pseudo-tetragonal Jahn–Teller distortion direction while the short distance of 1.98 Å approximately corresponds to the Mn^{IV}-O bond length. These results led us to an conclusion that the oxidation state of Mn2 fluctuates between +3 and +4 from time to time, resulting in the bond-length fluctuation along the pseudo-tetragonal Jahn–Teller distortion direction parallel to the a axis.

The fluctuation of oxidation states and bond lengths in the $Mn2_4O9_4$ heterocubane is presumably explained from the formation of Zener-type polaron in which three *e*-parentage electrons are shared by the four Mn atoms through the double-exchange Zener mechanism.[26),27)] This provides the time-averaged oxidation state of 3.25 for the Mn2 site. The *e*-parentage low-energy level orbitals of the four Mn atoms aligns along the a axis in an ordered way and accommodate 3/4 electron per orbital in time-average. This results in the appearance of a weak Jahn–Teller distortion along the a axis. In a viewpoint of a fully ionic picture, there are three Mn^{III} and one Mn^{IV} in the heterocubane while their charges swap as a function of time. The charge swapping simultaneously causes the appearance/disappearance of pseudo-tetragonal Jahn–Teller distortion, resulting in the oscillation of the four O9 atoms of the heterocubane. The other four counterpart O4 atoms coordinated to the Mn atoms are also involved in this dynamical Jahn–Teller distortion but the degree is less prominent than the O9 atoms because the O4 atoms are also bonded to two Mn and one Li atoms with fixed (time-independent) charges.

4. Partial charge ordering and Zener polarons

The partial charge ordering in the low-temperature modification can be summarized as below. There are five Mn sites, i.e.,

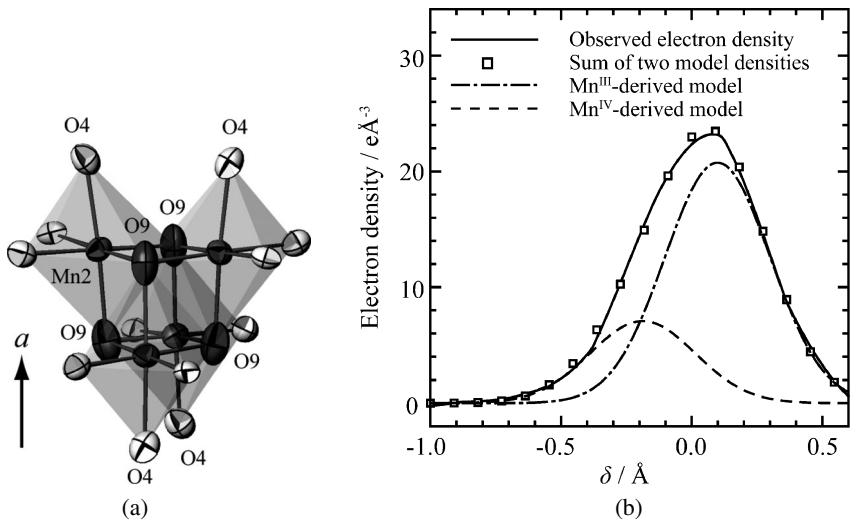

Fig. 4. Four $Mn2O_6$ octahedra capping a tetrahedral void composed of four O9 atoms (a) and the electron density distribution of O9 at 297 K (b) as a function of δ(Å), the distance along the a axis from the refined O9 atom position (Mn2 is located at negative δ). Figure 4(b) consists of the observed asymmetric electron density distribution (solid line) around O9, Gaussian model density (dash-dotted line) assuming Mn^{III} at 2.24 Å, Gaussian model density (dashed line) assuming Mn^{IV} at 1.98 Å, and the sum of two models (square marks).

Mn1(16), Mn2(32), Mn3(32), Mn4(32), and Mn5(32), where the figure in parentheses stands for the number of sites in a unit cell. All Mn atoms except for those at Mn2 sites are almost perfectly charge-ordered. Mn1 and Mn3 sites are in the oxidation state of +3 while Mn4 and Mn5 sites are +4. The undegenerate *e*-parentage low-energy-level orbitals of Mn1 and Mn3 accept one electron and the distortions align along the *c* and *b* axes, respectively. The low-energy-level undegenerate *e*-parentage orbitals at four Mn2 sites in $Mn2_4O9_4$ cluster are orbitally-ordered along the *a* axis while not charge-ordered, because one electron is missing to fill these orbitals. The one missing electron, i.e., a hole, is trapped within the heterocubane, and is considered as neither itinerant nor localized, but somewhere in between. There are 32 Mn2 sites in a unit cell, among which 24 Mn^{III} and 8 Mn^{IV} exist as a snap shot of time. Considering the oxidation states of all other Mn atoms, the ratio of Mn^{III} and Mn^{IV} becomes 1:1, which fulfills the electrical neutrality condition for $LiMn_2O_4$. As shown in **Fig. 5**, the heterocubane Zener polarons are spatially ordered with their polar axes aligned along the *a* axis in the low temperature modification.

The $3 \times 3 \times 1$ superstructure as shown in **Fig. 6** has similar cell dimensions along the *a* and *b* axes and the *Fddd* space group places no symmetry difference along these directions. If Mn1, Mn2 and Mn3 take the same oxidation state of +3 and exert to an equal magnitude the pseudo-tetragonal Jahn–Teller distortion

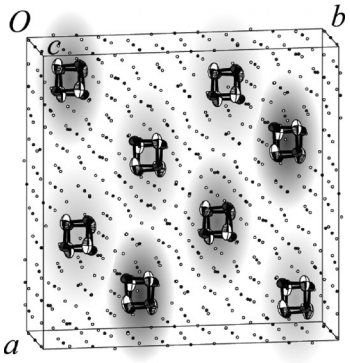

Fig. 5. Ordered distribution of $Mn2_4O9_4$ heterocubane Zener polarons in the low-temperature modification. The shade of polarons indicates the depth along the *c* axis.

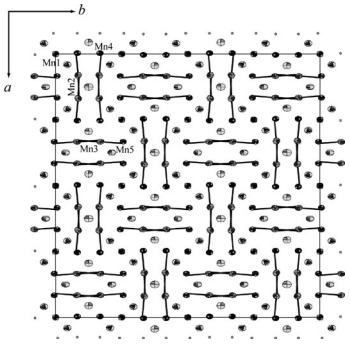

Fig. 6. Unit cell structure of the low-temperature modification viewed along the *c* axis, depicting the elongated pseudo-tetragonal Jahn–Teller bonds of Mn2–O (nearly parallel to the *a* axis) and Mn3–O (nearly parallel to the *b* axis). The Mn1–O pseudo-tetragonal Jahn–Teller bonds lie nearly parallel to the *c* axis.

along *c*, *a*, and *b*, respectively, then the structure has no reason to crystallize in orthorhombic instead of tetragonal. The little difference in *a* and *b* cell dimensions evidences the difference in magnitude of pseudo-tetragonal Jahn–Teller distortion between $Mn2O_6$ and $Mn3O_6$. The ordered appearance of the heterocubane Zener polarons along the *a* axis in the low temperature modification is thus considered as an origin of orthorhombicity.

The spinel-type structure is known as a frustrated system in a sense that the alternate arrangement of octahedrally-coordinated transition metal atoms with different electron configuration cannot be allowed topologically. This structural constraint could be a reason for the appearance of such complex structure in the low-temperature modification of $LiMn_2O_4$. The hole trapping within a limited local space like $Mn2_4O9_4$ heterocubane cluster and the appearance of bond-length fluctuation seem a solution for ordering other Mn valences in the remaining voluminous part of structure at low temperatures. The partial charge ordering in the low temperature modification can be thus rationalized.

The existence of heterocubane Zener polarons in the high-temperature modification is not evidenced so far experimentally. If they do exist, they are not ordered but probably migrate over the tetrahedral voids in the structure as a function of time. The phase transition in $LiMn_2O_4$ seems better described from a view point of sudden appearance of the ordered heterocubane Zener polarons at low temperatures, or the order/disorder transition of the heterocubane Zener polarons. By replacing the Mn atoms partially with other metal atoms like Mg, the cubic symmetry becomes stabilized throughout the temperature range required for practical application.[28)–31)] An increase in the number of dopants will hinder the concerted phenomenon in the formation of the heterocubane Zener polaron or its ordering at low temperatures. For these reasons, the replacement of Mn with other elements is considered as effective in stabilizing the cubic phase.

5. Positional disorder in the high-temperature modification

Molecular dynamics (MD) simulation was carried out at various temperatures using MXDORTO[32)] at 2 fs intervals. The Verlet algorism with NTP ensemble at a room pressure of 0.1 MPa was employed.[33)] The MD cell of $4 \times 4 \times 4$ crystallographic unit cells was used with the P1 symmetry. The effective charges were assumed as +1 for Li, +1.4 for Mn^{III}, +2.4 for Mn^{IV}, and –1.2 for O. The potential function used was of Gilbert-Ida type.[34),35)] The 16*d* sites are assumed to be occupied by Mn^{III} and Mn^{IV} in equal numbers. They are distributed using the random number table before commencing the simulation (model I). The initial structure became fully relaxed 30 ps after the commencement of simulation.

It was believed that the Li atom diffusion in $LiMn_2O_4$ is a simple hopping over 8*a* and 16*c* sites along the zigzagging chain as shown in Fig. 1.[6),16)] However, the spatial distribution of Li atoms at 300 K becomes rather complex as shown in **Fig. 7**. Some Li atoms are even outside the coordination tetrahedra. The frequency distribution of Li atoms along the diffusion pathway on the (–110) section (Fig. 7) suggested that ca. 90% of Li atoms are located near any one of the four available positions (B in Fig. 7) which are ca. 0.16 Å displaced from 8*a*, while the remaining 10% atoms move out of the originally located tetrahedron and reside in a relatively broad area (A in Fig. 7) 0.2–0.5 Å displaced from 16*c*. The distribution of Li atoms obtained from the MD simulation is consistent with the X-ray results as shown in Fig. 3.

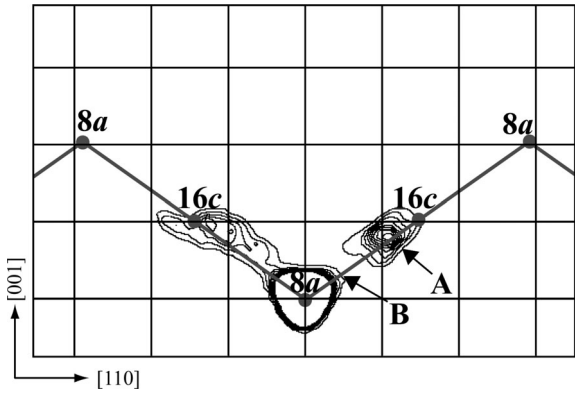

Fig. 7. Two-dimensional distribution of Li atoms on (–110) obtained from the MD calculation (model I) in the same area as that given in Fig. 3. Contours are truncated near the 8*a* site.

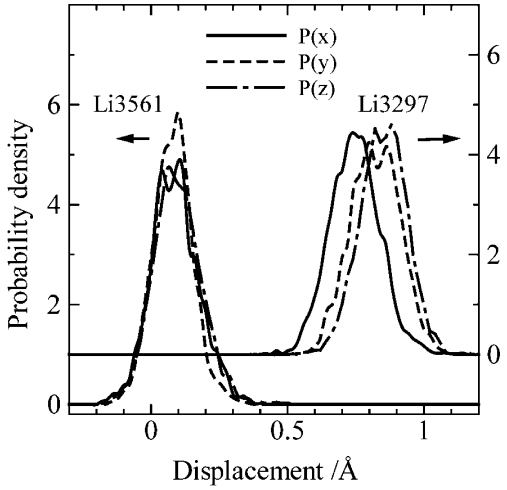

Fig. 8. Probability density distributions, $P(x)$, $P(y)$ and $P(z)$ of Li3561 and Li3297 atoms as a function of displacement from the ideal 8*a* site.

6. Thermal vibration

Figure 8 shows the probability density distribution of two Li atoms numbered Li3297 and Li3561 in the MD cell. The statistics were obtained in the time period between 100 and 120 ps in the MD simulation. Li3561 is slightly displaced from the ideal 8*a* site (zero displacement position in abscissa) in its coordination tetrahedron, while Li3297 has hopped out from the tetrahedron with a displacement magnitude of ca. 0.8 Å. The *x*, *y* and *z* components of the probability density distribution can be approximated by the Gaussian function, indicating that Li atoms vibrate harmonically at their equilibrium positions which are not necessarily identical with the regular position like 8*a*. The same was true for the O atoms. They vibrate harmonically at their equilibrium positions slightly displaced from the 32*e* sites. It is noted that this phenomenon is observed under the condition that the oxidation states of Mn have not been modified throughout the simulation (model I).

7. Effect of redistribution of Mn valences on the Li atom distribution

Random walk theory tells that the mean square displacement (MSD) of a particle in diffusion increases linearly as a function

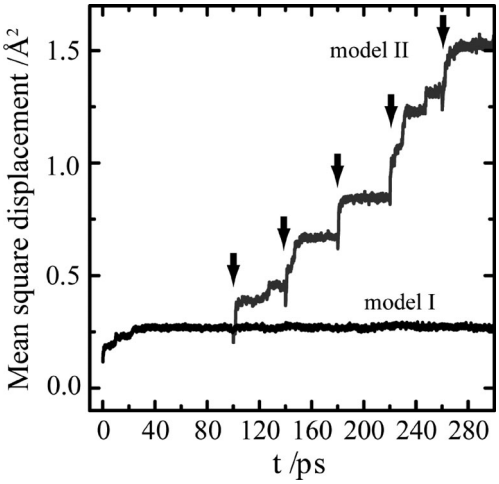

Fig. 9. Changes in the mean square displacements of Li atoms with time in model I, assuming the random and time-independent distribution for Mn valences, and model II, assuming the random and time-dependent distribution for Mn valences.

of time. As shown in **Fig. 9**, the MSD of Li atom in model I becomes constant against time after the relaxation period is over. This means that the model I does not explain well the Li atom diffusion at 300 K. Actually, Li atoms cannot go further than the neighbors of 16*c*, as shown in Fig. 7.

Distortion of the LiO_4 tetrahedron is strongly affected by the oxidation states of 12 Mn atoms in the second shell centered at 8*a*. To find the effect of oxidation states of Mn on the Li atom diffusion, the Mn valences are re-distributed using the random number table at 40 ps intervals after the first 100 ps relaxation period is over (model II). The Li atoms start to move immediately after changing the valences of nearby Mn atoms and relaxed at their new positions within 10–20 ps. Accordingly, the MSD of Li increases stepwise as a function of time, as shown in Fig. 9. The model II simulation exemplifies that (1) changes in Mn valences prompt the O atom displacements, (2) displacements of the O atoms affect seriously the coordinated Li atom positions, (3) once the Li atoms have moved to their new stable positions, they vibrate harmonically and do not move further, (4) to break harmonic vibration of Li at the equilibrium position, changes in Mn valences are necessary, (5) redistribution of Mn valences at an appropriate interval can virtually present the situation in which the Li cations continuously (though still discrete in a finer time scale) diffuse in three-dimensional directions. The distribution of Li atoms along the diffusion pathway is shown in **Fig. 10** after when Mn valences are redistributed 5 times (model II) in comparison with zero times (model I). It can be seen that the Li atom diffusion has progressed much further by repeating the redistribution procedure.

8. Bottleneck size

The bottleneck geometry is a measure to estimate the ease of diffusion since a local maximum (saddle point) of the potential curve is usually formed at the bottleneck for diffusion species. The bottleneck geometry changes as a function of time because of atomic vibration and some other factors. In this respect the time-resolved structure obtained from the MD simulation can provide useful information about diffusion through the bottleneck.

In $LiMn_2O_4$, the bottleneck is the oxygen triangle formed at

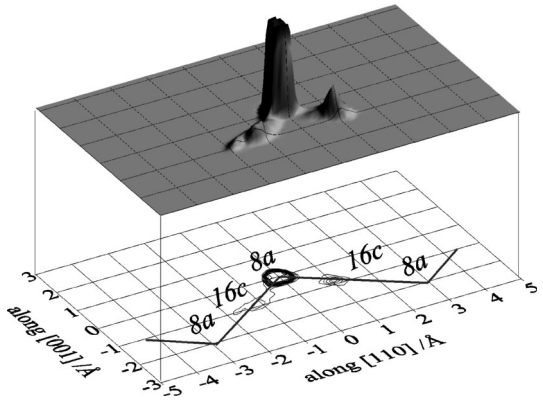

(a)

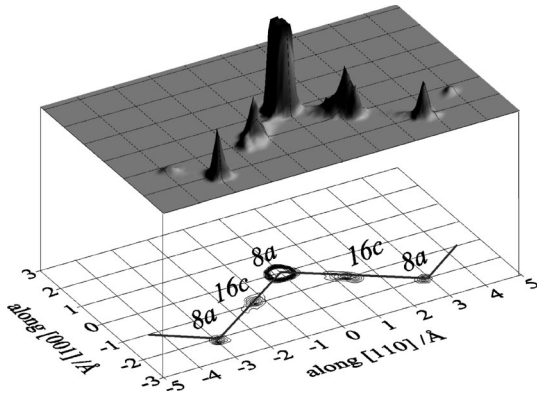

(b)

Fig. 10. Two-dimensional distributions of Li atoms on (110) with the zigzagging diffusion pathway connecting 8*a*-16*c*-8*a* sites obtained from the MD simulation for (a) model I and (b) model II.

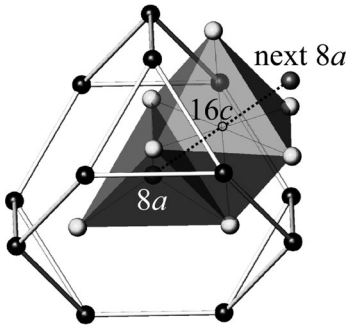

Fig. 11. First and second nearest coordination shells around 8*a* and 16*c* in $LiMn_2O_4$.

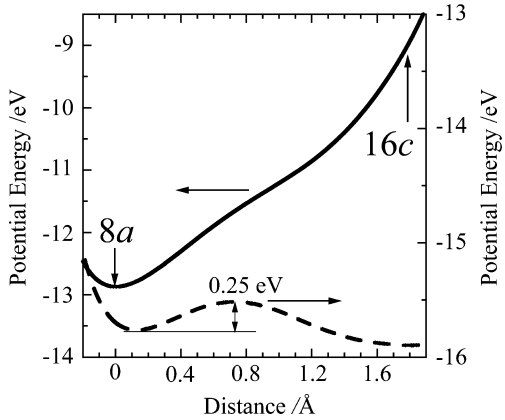

Fig. 12. Potential curves of Li3392 in the MD cell as a function of distance from 8*a* toward 16*c* assuming the mean field approximation for Mn valences. The solid line is for the model in which neighboring two 8*a* sites are occupied by Li. The dashed line is for the model in which Li is absent at the next nearest 8*a* site.

the contact face between the tetrahedron about 8*a* and the octahedron about 16*c*. The radius of circumscribed circle of the oxygen triangle can be taken as the bottleneck size. The statistics of the MD simulation shows that the bottleneck size is 1.987(14) Å in average when Li succeeds in passing through it. The value is slightly larger than 1.97 Å, the sum of ionic radii of Li^+ (0.59 Å) and O^{2-} (1.38 Å).[7] When Li is confined to the tetrahedron, the bottleneck size is 1.903(2) Å in average, which is clearly much smaller than the sum of ionic radii. This suggests that the possibility of Li atom to hop out from its coordination tetrahedron is quite small at 300 K unless the bottleneck is enlarged by displacements of the O atoms.

9. Diffusion mechanism of Li atoms

We first discuss results obtained from the mean field approximation in which all the Mn valences are assumed as +3.5. **Figure 11** shows the local structure around the straight line connecting the 8*a*-16*c*-8*a* sites. If both 8*a* sites are occupied by Li, as is normal for the ideally stoichiometric structure, the potential curve monotonically increases from 8*a* to 16*c* as shown in **Fig. 12**. The stable site is 8*a*. On the other hand, if one of the two 8*a* sites is empty, then the potential curve is modified to the dashed one in Fig. 12. The 16*c* site is 0.15 eV more stable than the metastable 8*a* site. The potential curve has a saddle point at the bottleneck, and an activation energy of ca. 0.25 eV is necessary to jump from 8*a* to 16*c* across the saddle point. This situation can be regarded as a microscopic version of the classical diffusion mechanism based on the concentration difference of diffusion species.

Given that the Mn atoms take discrete oxidation states of +3 and +4, the mean field approximation may not be fully appropriate. An example is given in **Fig. 13**. The second shell of the 16*c* site contains a 6-membered ring of Mn atoms. If the ring is composed of 4 Mn^{III} and 2 Mn^{IV}, then the potential has a minimum at a position close to 16*c* while the tetrahedral 8*a* site becomes unstable before and after the jump. There is no saddle point to require an activation energy for diffusion. The potential energy at the local minimum is ca. 1.0 eV lower than 8*a*. The location of the local minimum has a small offset from 16*c* due to the presence of Li at the next 8*a* site in the opposite side.

As shown in Fig. 11, the first coordination shell about 8*a* is composed of 4 O atoms at 1.93 Å in a tetrahedral arrangement. The second shell is composed of 12 Mn at 3.41 Å, 12 O at 3.44 Å and 4 Li at 3.56 Å. The second shell is thus located far from 8*a* and the electrical condition of the shell is relatively neutral. On the other hand, the first shell of the 16*c* interstice is composed of 2 Li atoms at 1.78 Å and 6 O atoms at 2.14 Å. The second shell is composed of 6 Mn atoms in the shape of 6-membered ring at 2.91 Å and 8 O atoms at 3.5–3.7 Å. The 2nd shell of the 16*c* interstice has a strong directional dependency in the electrostatic field. The potential curve along the diffusion pathway is thus susceptible to the changes in Mn valences composing the 6-membered ring in the 2nd shell.

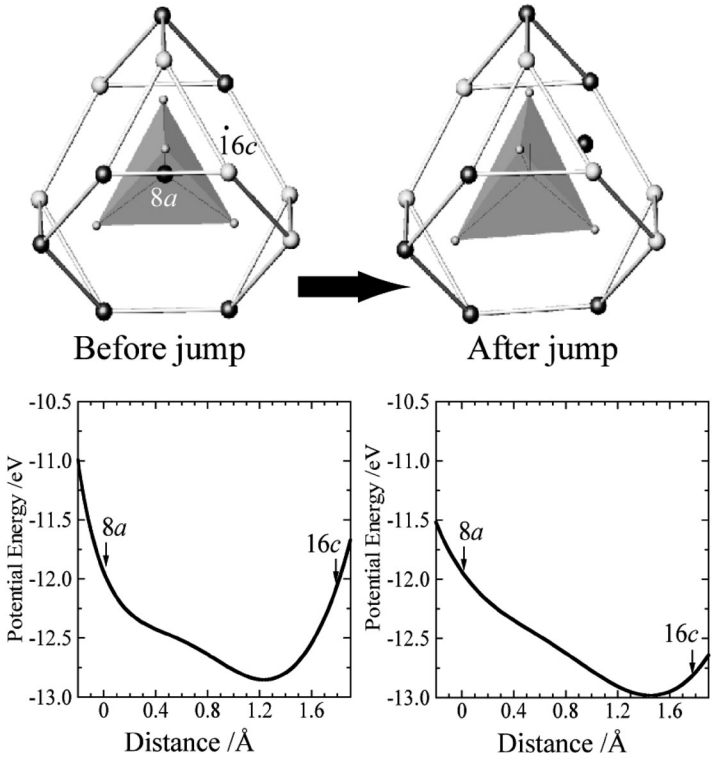

Fig. 13. Potential curves of Li3308 in the MD cell as a function of distance from 8*a* toward 16*c* before (left) and after (right) the Li-hop when the 6-membered Mn ring in the second nearest shell about 16*c* is composed of 4 Mn^{III} (light grey) and 2 Mn^{III} (dark grey).

The effect of charge distribution of the 6-membered Mn ring on the probability of Li presence at 16*c* was investigated from the MD statistics. A large difference was found between the two cases, i.e., one is the normal situation where 16*c* interstice is empty, and the other is a situation where the 16*c* interstice is temporarily occupied by Li. The mean oxidation states of the 6-membered Mn ring were 3.5 for the former and 3.3 for the latter. The value of 3.3 corresponds typically to the case in which the ring is composed of 4 Mn^{III} and 2 Mn^{IV}. Recalling that the mean oxidation state of the 6-membered Mn ring is 3.5 for the random and even distribution of Mn^{III} and Mn^{IV}, the value of 3.3 corresponds to a situation where an electron is donated to the ring. The donor is Mn^{III} in the neighbor of the ring. This situation can be reworded as; the Li atom can hop from 8*a* to 16*c* interstice when one Mn^{IV} atom in the 6-membered Mn ring is reduced to Mn^{III} by accepting an electron from outside the ring.

This second diffusion mechanism is different from the aforementioned microscopic version of the classical picture for diffusion driven by the concentration difference in chemical species. The driving force in the second mechanism is associated with the 3*d* electron transfer in the *e*-parentage orbitals of nearby Mn atoms. The 3*d* electrons can hop over Mn atoms via the thermal activation process or the double exchange interaction. Swapping the charges between nearby heterovalent Mn pair modulates surrounding O atom positions, opens the bottleneck, lowers the potential of the 16*c* interstice, and finally displaces Li from 8*a* to a position close to 16*c*. It is stressed again that the Li atom diffusion associates with the dynamics of the local electron-lattice interaction.

10. Comparison with the olivine-type Li_xFePO_4

Recent development of Li_xFePO_4 as the positive electrode in the large-scale battery for motor vehicles may drive away the cobaltite and manganite materials like Li_xCoO_2 and $Li_xMn_2O_4$ due to cost and safety reasons. $Li_xMn_2O_4$ tends to decompose and release oxygen gas at elevated temperatures. The oxygen gas and the flammable organic solvent in electrolyte can cause battery fires because of unexpected heat on overcharge. The O atoms in the olivine-type Li_xFePO_4 seem more firmly bound to the skeleton owing to the presence of the short tetrahedral P–O bonds with covalent nature of *ca.* 1.54 Å. This structural property can reduce the problem of oxygen gas generation, compared with the octahedrally-coordinated skeletons in cobaltites and manganites. On the other hand Li_xFePO_4 is less conductive in electronic and ionic points of view because the Li ion vacancy and Fe^{III} pair is strongly coupled and less mobile. In the extraction/insertion cycles of Li in Li_xFePO_4 ($0 \leq x \leq 1$), the electron hopping between Fe^{II} and Fe^{III} plays an important role in the Li atom diffusion as is the case for $LiMn_2O_4$. To overcome the poor mobility of electrons over Fe atoms and the associated low ionic conductivity in the Li_xFePO_4 bulk crystal, various energetic surveys have been done including particle size reduction, doping, carbon nano-coating, etc. The results are not only promising for practical applications but also fruitful for deeper understandings of the structural chemistry of Li_xFePO_4. Since summarizing a huge number of the recent state-of-the-art papers on $LiFe_xPO_4$ is out of scope of this short review, only the selected ones are indicated in the list of references for readers.[36)–40)]

11. Closing remarks

The Li atom diffusion in $LiMn_2O_4$ was thought to be a simple hopping over the tetrahedral 8*a* sites and octahedral 16*c* interstices along the diffusion pathway. However, the precise X-ray experiments and MD simulations revealed that there are many more positions available for Li to reside. The ideal positions of 8*a* (1/8,1/8,1/8) and 16*c* (0,0,0) are unstable rather than these.

Dynamical distortion of the oxygen tetrahedron surrounding the Li atom is necessary to make it diffuse because of the slightly small bottleneck size. The electron transfer among the *e*-parentage orbitals of Mn atoms induces a dynamic deformation of the LiO_4 tetrahedra. The electron transfer and the Li atom hop presumably occur concomitantly, mediated by a local deformation of lattice. Two kinds of diffusion mechanisms have been worked out. One is a microscopic version of the traditional diffusion based on the concentration difference in diffusion species. This requires an activation energy of ca. 0.25 eV to jump over a saddle point at the bottleneck. The other is a diffusion accompanied by the local lattice distortion coupled with the 3*d* electron transfer. This requires no activation energy for Li to pass through the bottleneck.

Regarding the diffusion of atoms in solid, a stereotyped image would be a simple hopping along the diffusion tunnel with firm wall under the gradient of its chemical potential. However more likely we would realize that the tunnel walls in $LiMn_2O_4$ are much flexible rather than firm. Not only the Li atoms move by themselves but also they are forced to move by the peristaltic deformation of the diffusion tunnel, which is invoked by the dynamic behavior of the 3*d* electrons of Mn atoms shrouded in the $[Mn_2O_4]^{-1}$ matrix.

Acknowledgements We thank Prof. M. Wakihara, Prof. S. Oishi, Dr. D. du Boulay, Dr. J. R. Hester, Dr. Y. Tabira, Dr. S. Kishimoto, Dr. S. Kuze, Dr. Y. Matsushima, Ms. K. Suda and Mr. M. Hayatsu for their help in experiments and calculations. The work is supported by Grants-in-Aid for Scientific Research No. 18206071 from Japan Society of Promotion of Science. Synchrotron X-ray experiments were carried out at KEK-PF under the programs, No. 2004G037, 2007G027 and 2007G028. Part of the work was done at the Materials and Structures Laboratory, Tokyo Institute of Technology, to which the authors thanks are due.

References

1) J. B. Goodenough, M. M. Thackery, W. I. F. David and P. G. Bruce, *Rev. Chim. Miner*, 21, 435–455 (1984).
2) T. Ohzuku, M. Kitagawa and T. Hirai, *J. Electrochem. Soc.*, 137[3], 769–774 (1990).
3) J. M. Tarascon, E. Wang, F. K. Shokoohi, W. R. Mckinnon and S. Colson, *J. Electrochem. Soc.*, 138[10], 2859–2863 (1991).
4) D. Guyomard and J. M. Tarascon, *J. Electrochem. Soc.*, 138[10], 2864–2868 (1991).
5) A. Mosbah, A. Verbaere and M. Tournoux, *Mat. Res. Bull.*, 18[11], 1375–1381 (1983).
6) M. Wakihara, *Materials Science and Engineering*, R33, 109–134 (2001).
7) R. D. Shannon, *Acta Crystallogr. Sect. A*, A32, 751–767 (1976).
8) B. Ammundsen, J. Roziere and M. S. Islam, *J. Phys. Chem. B*, 101, 8163–8165 (1997).
9) A. Yamada and M. Tanaka, *Mater. Res. Bull.*, 30[6], 715–721 (1995).
10) Y. Shimakawa, T. Numata and J. Tabuchi, *J. Solid State Chem.*, 131, 138–143 (1997).
11) J. Rodriguez-Carvajal, G. Rousse, C. Masquelier and M. Hervieu, *Phys. Rev. Lett.*, 81[21], 4660–4663 (1998).
12) K. Oikawa, T. Kamiyama, F. Izumi, B. C. Chakoumakos, H. Ikuta, M. Wakihara, J. Li and Y. Matsui, *Solid State Ionics*, 109, 35–41 (1998).
13) H. Yamaguchi, A. Yamada and H. Uwe, *Phys. Rev. B*, 58, 8–11 (1998).
14) G. Rousse, C. Masquelier, J. Rodríquez-Carvajal and M. Hervieu, *Electrochemical and Solid-State Letters*, 2, 6–8 (1999).
15) M. Tachibana, T. Tojo, H. Kawaji, T. Atake, M. Yonemura and R. Kanno, *Physical Review B*, 68[9], 094421 (2003).
16) V. W. J. Verhoeven, I. M. de Schepper, G. Nachtegaal, A. P. M. Kentgens, E. M. Kelder, J. Schoonman and F. M. Mulder, *Phys. Rev. Lett.*, 86[19], 4314–4317 (2001).
17) N. Ishizawa, D. du Boulay, M. Hayatsu, S. Kuze, Y. Matsushima, H. Ikuta, M. Wakihara, Y. Tabira and J. R. Hester, *J. Solid State Chem.*, 174, 167–174 (2003).
18) K. Tateishi, D. du Boulay, N. Ishizawa and K. Kawamura, *J. Solid State Chem.*, 174, 175–181 (2003).
19) K. Tateishi, D. du Boulay and N. Ishizawa, *J. Cerm. Soc. Japan*, 112[5], S658–S662 (2004).
20) K. Tateishi, K. Suda, D. du Boulay, N. Ishizawa and S. Oishi, *Acta Crystallogr. Sect. E*, E60, i18–i21 (2004).
21) K. Tateishi, PhD thesis, Tokyo Institute of Technology (2005) [in Japanese].
22) K. Tateishi, D. du Boulay and N. Ishizawa, *Appl. Phys. Lett.*, 84[4], 529–531 (2004).
23) N. Ishizawa and K. Tateishi, *J. Cryst. Soc. Jpn.*, 48, 17–24 (2006) [in Japanese].
24) Y. Satow and Y. Iitaka, *Rev. Sci. Instrum.*, 60, 2390–2393 (1989).
25) S. Kishimoto, N. Ishizawa and T. P. Vaalsta, *Rev. Sci. Instrum.*, 69, 384–391 (1998).
26) C. Zener, *Phys. Rev.*, 82, 403 (1951).
27) J. Goodenough, "Magnetism and the Chemical Bond," John Wiley and Sons, New York (1963).
28) R. J. Gummow, A. de Kock and M. M. Thackeray, *Solid State Ionics*, 69, 59–67 (1994).
29) C. Sigala, D. Guyomard, A. Verbaere, Y. Piffard and M. Tournoux, *Solid State Ionics*, 81, 167–170 (1995).
30) L. Guohua, H. Ikuta, T. Uchida and M. Wakihara, *J. Electrochem. Soc.*, 143, 178–182 (1996).
31) G. Piostoia, A. Antonini, R. Rosati and C. Bellitto, *J. Electroanal. Chem.*, 410, 115–118 (1996).
32) K. Kawamura, MXDORTO: Japan Chemistry Program Exchange, #026.
33) L. Verlet, *Phys. Rev.*, 159, 98–103 (1967).
34) Y. Ida, *Physics of the Earth and Planetary Interiors*, 13, 97–104 (1976).
35) K. Suzuki, Y. Oumi, S. Takami, M. Kubo, A. Miyamoto, M. Kikuchi, N. Yamazaki and M. Mita, *Jap. J. of Appl. Phys.*, 39, 4318–4322 (2000).
36) A. K. Padhi, K. S. Nanjundaswamy and J. B. Goodenough, *J. Electrochem. Soc.*, 144, 1188–1194 (1997).
37) A. Yamada, H. Koizumi, S. Nishimura, N. Sonoyama, R. Kanno, M. Yonemura, T. Nakamura and Y. Kobayashi, *Nature Materials*, 5, 357–360 (2006).
38) C. Delmas, M. Maccario, L. Croguennec, F. Le Cras and F. Weill, *Nature Materials*, 7, 665–671 (2008).
39) S. Nishimura, G. Kobayashi, K. Ohoyama, R. Kanno, M. Yashima and A. Yamada, *Nature Materials*, 7, 707–711 (2008).
40) P. Gibot, M. Casas-Cabanas, L. Laffont, S. Levasseur, P. Carlach, S. Hamelet, J.-M. Tarascon and C. Masquelier, *Nature Materials*, 7, 741–747 (2008).

Nobuo Ishizawa received his degree of Dr. Sci. & Eng. from Tokyo Institute of Technology in 1979. Subsequently as a Research Associate at the Faculty of Engineering, and as an Associate Professor at Research Laboratory of Engineering Materials (Materials and Structures Laboratory) in Tokyo Institute of Technology, he conducted crystallographic studies on functionally-important inorganic materials. He is a Professor at Ceramics Research Laboratory, Nagoya Institute of Technology.

Kenji Tateishi received his degree of Dr. Sci. & Eng. from Tokyo Institute of Technology on the crystallographic study of lithium manganite in 2005. Subsequently he has been engaged in the development of ceramic materials at Gifu Prefectural Ceramics Research Institute.